Recover certain low-frequency information for full waveform inversion

Xiao-Bi Xie Institute of Geophysics and Planetary Physics, University of California at Santa Cruz*

Summary

In full waveform inversion, it is preferred to use the multi-scale approach which starts iteration from low-frequency data to determine the large-scale heterogeneities first. This approach tends to provide better convergence when the initial model is drastically biased from the true velocity model. However, the combined passband of the source and geophone usually generates data lacks the low-frequency information preferred by the full waveform inversion. On the other hand, the travel time data are often used to generate low-resolution initial models. The low-frequency waveform and the travel-time information share some common properties. The successful use of travel time data implies that the seismic data are weakly dispersed at least at low frequencies. This property can be used to extrapolate the phase information in the data towards lower frequencies. Motivated by this idea, we propose a method to convert high-frequency waveforms into low-frequency waveforms based on a linear phase approximation at the low frequency end. The resulted low-frequency waveform can benefit the convergence in full waveform inversion. To validate the proposed method, we compare waveforms converted from high-frequency traces with those actually generated using low-frequency sources. We successfully tested the converted data set in waveform inversion. The inversion using the high-frequency converted low-frequency seismic data converge better than those directly using the original high-frequency data.

Introduction

The full waveform inversion (FWI) in searching for the correct velocity model is intrinsically nonlinear. To bypass this difficulty, the nonlinear problem is often linearized and solved by linear inversions in an iterative way. For linear inversions based on the perturbation theory, when the initial model is drastically biased from the true velocity model, the convergence is often a challenge. To solve this problem, many authors chose to start the inversion from low-frequency data. For the frequency-domain method, the inversion can be started from the lowest frequency component in the data, or use a group of frequencies at the lower end (Sirgue and Pratt, 2004; Operto et al., 2007; Ben-Hadj-Ali et al., 2008). For the time-domain method, the low frequency waveforms are used first (Bunks et al., 1995; Boonyasiriwat et al., 2009). The low-frequency information tends to sense the large-scale heterogeneities in the model. Although lacks the capability to constrain the fine-scale structures, we can use it to characterize long wavelength (large scale) components in the model. After determined the large-scale heterogeneities, we can turn to high-frequencies to determine small-scale heterogeneities in an iterative way. To apply this multi-scale inversion, the key point is having data with required low-frequency information. However, due to limited passband of the source and geophone, the information of a few Hz is often unavailable. Several authors searched for methods which can recover low-frequency information from the data (e.g., Fei and Luo, 2012).

On the other hand, the travel time information formed by accumulated multiple forward scattering shares many common properties with low-frequency waveforms. It senses mostly large-scale heterogeneities in the model and can be used to obtain a low-resolution (large scale) initial model for subsequent FWI. Usually, the travel time data are obtained by investigating the impulse traveling in the space-time, with the premise that the wave is not strongly dispersed, at least at the low frequencies. Otherwise, the impulse will be quickly distorted, making the travel time measurement impossible. Under the weak dispersion, wave components with different frequencies have nearly linear phase, i.e., the phase is approximately proportional to the frequency. Based on this approximation, if low-frequency phase information is missing in the data, we can linearly extrapolate the phase from higher frequencies and use it to rebuild the low-frequency part in the waveform. Based on this, we propose a method that can recover certain low-frequency information from the data.

Methodology

To introduce this method, we starting from analyze the spectra of high- and low-frequency waveforms. Shown on the top of Fig 1 are two synthetic seismograms calculated in the BP model. They are from the same source and receiver locations but trace (a) uses a 10-Hz Ricker wavelet and trace (b) uses a 3-Hz Ricker wavelet. The original waveforms are sampled with a short time window (shown on the time axis) and the sampled waveforms are illustrated under the original waveforms. Then they are transformed into the frequency domain shown as (c) and (d), where from left to right are their amplitude, phase and unwrapped phase spectra. After sampled by a short time window, both the amplitude and phase spectra are simple. Particularly, the phase spectrum becomes regular and can be easily unwrapped. At low frequencies, the unwrapped phases for both high- and low-frequency waveforms are similar and close to linear dispersion, indicating if the phase information at lower frequencies is missing, it may be approximated by linearly extrapolating the high-frequency dispersion curve.

DOI http://dx.doi.org/10.1190/segam2013-0451.1

Following the above analysis, we present our approach. By applying a short time window $W(t)$ to a seismogram generated from a high-frequency source, we obtain a short waveform $f_H(t)$. We discuss how to convert $f_H(t)$ to a waveform $f_L(t)$, as could be obtained by similarly sampling a seismogram from a low-frequency source. In the frequency domain, both traces can be expressed as

$$f_L(\omega) = R(\omega)\cdot\left[S_L(\omega) * W(\omega)\right] \quad (1)$$

$$f_H(\omega) = R(\omega)\cdot\left[S_H(\omega) * W(\omega)\right] \quad (2)$$

where $R(\omega)$ is the response of the earth, $S(\omega)$ is the nominal source spectrum but actually composed of effects from both source and the geophone response, $W(\omega)$ is the spectrum of the sampling window, the asterisk denotes the convolution, and the subscripts L and H denote the low-frequency and high-frequency traces. It appears we can simply apply a convolution/deconvolution operator

$$C(\omega) = \frac{S_L(\omega) * W(\omega)}{S_H(\omega) * W(\omega)} \quad (3)$$

on $f_H(\omega)$ to convert it into $f_L(\omega)$. However, due to the lack of useful low-frequency information in $S_H(\omega)$, using operator 3 is impractical.

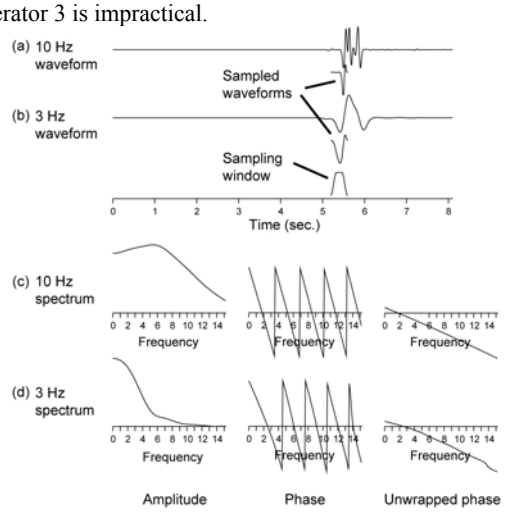

Fig 1. Comparison between 10-Hz and 3-Hz waveforms, and their amplitude and phase spectra. Note a short sampling window is applied to the waveform before the Fourier transform.

To bypass this difficulty, we first separate these spectra into amplitude spectrum $A(\omega)$ and phase spectrum $\varphi(\omega)$

$$f_L(\omega) = A_L(\omega)\exp\left[i\varphi_L(\omega)\right], \quad (4)$$

$$f_H(\omega) = A_H(\omega)\exp\left[i\varphi_H(\omega)\right]. \quad (5)$$

Then, separate all spectra into their low-frequency parts and high-frequency parts,

$$A_L(\omega) = \left[A_L^l(\omega), A_L^h(\omega)\right]\begin{bmatrix} w^l(\omega) \\ w^h(\omega)\end{bmatrix}, \quad (6)$$

$$\varphi_L(\omega) = \left[\varphi_L^l(\omega), \varphi_L^h(\omega)\right]\begin{bmatrix} w^l(\omega) \\ w^h(\omega)\end{bmatrix}, \quad (7)$$

$$A_H(\omega) = \left[A_H^l(\omega), A_H^h(\omega)\right]\begin{bmatrix} w^l(\omega) \\ w^h(\omega)\end{bmatrix}, \quad (8)$$

$$\varphi_H(\omega) = \left[\varphi_H^l(\omega), \varphi_H^h(\omega)\right]\begin{bmatrix} w^l(\omega) \\ w^h(\omega)\end{bmatrix}, \quad (9)$$

where superscripts *l* and *h* denote the low-frequency part and high-frequency part of the spectra, and $w^l(\omega)$ and $w^h(\omega)$ are weighting functions over frequency. $w^l(\omega)$ is zero at high-frequency band and $w^h(\omega)$ is zero at low-frequency band. In the intermediate frequencies, they have certain overlaps, and $w^l(\omega) + w^h(\omega) = 1$. Their crossover frequency is determined by the available low-frequency content in the data. Below the crossover frequency, $f_H(\omega)$ is dominated by noise.

Assuming that, in $f_H(\omega)$, the low-frequency part $A_H^l(\omega)$ and $\varphi_H^l(\omega)$ are either too noisy or totally missing, but their high-frequency contents $A_H^h(\omega)$ and $\varphi_H^h(\omega)$ are reliable, our target is using these high-frequency contents to rebuild (or estimate) a new data $f_L(\omega)$, i.e., to determine $A_L^l(\omega)$, $A_L^h(\omega)$, $\varphi_L^l(\omega)$, and $\varphi_L^h(\omega)$. We first create source models $\left|S_H(\omega) * W(\omega)\right|_M$ and $\left|S_L(\omega) * W(\omega)\right|_M$ for the original and targeted waveforms, where subscript *M* denotes the model. If original waveform is from synthetics, we can simply adopt the known source function such as a Ricker wavelet for $S_H(\omega)$. If we are dealing with field data, $S_H(\omega)$ can be obtained by analyzing the frequency content of the data or by best fitting the data spectrum with a known source function. The $S_L(\omega)$ is determined by the targeted waveform, for example, we can choose a low-frequency Ricker source. Note we only need the amplitude of the source model. With these source models, we can convert $A_H^h(\omega)$ to $A_L^h(\omega)$ using

$$A_L^h(\omega) = \frac{\left|S_L(\omega) * W(\omega)\right|_M}{\left|S_H(\omega) * W(\omega)\right|_M} A_H^h(\omega). \quad (10)$$

For phase spectrum $\varphi_L^h(\omega)$, we directly use $\varphi_H^h(\omega)$, i.e.,

$$\varphi_L^h(\omega) = \varphi_H^h(\omega) \quad (11)$$

DOI http://dx.doi.org/10.1190/segam2013-0451.1

Based on the weak dispersion and linear phase property at low-frequencies, we linearly extrapolate the low-frequency end of $\varphi_H^h(\omega)$ to obtain $\varphi_L^l(\omega)$, i.e.,

$$\varphi_L^l(\omega) \xleftarrow[\text{Linear extrapolate}]{} \varphi_H^h(\omega). \quad (12)$$

Finally, we use the $A_L^h(\omega)$ from equation 9 and the source model $|S_L(\omega)*W(\omega)|_M$ to estimate the $A_L^l(\omega)$.

$$A_L^l(\omega) = \frac{|S_L(\omega)*W(\omega)|_M}{|S_L(\omega)*W(\omega)|_M^l} \cdot \frac{\overline{|S_L(\omega)*W(\omega)|_M^l}}{\overline{|S_L(\omega)*W(\omega)|_M^h}} \cdot \overline{A_L^h(\omega)}, \quad (13)$$

where $|S_L(\omega)*W(\omega)|_M \Big/ |S_L(\omega)*W(\omega)|_M^l$ is the normalized source model, which determine the shape of the spectral amplitude, $\overline{|S_L(\omega)*W(\omega)|_M^l} \Big/ \overline{|S_L(\omega)*W(\omega)|_M^h}$ is the ratio relating the low- and high-frequency average amplitudes of the source model, $\overline{A_L^h(\omega)}$ is the average amplitude of the high-frequency spectrum $A_L^h(\omega)$, the bar over variables denotes averaging, The averages in equation 13 can be calculated as

$$\overline{|S_L(\omega)*W(\omega)|_M^l} = \frac{\int |S_L(\omega)*W(\omega)|_M w^l(\omega)d\omega}{\int w^l(\omega)d\omega}, \quad (14)$$

$$\overline{|S_L(\omega)*W(\omega)|_M^h} = \frac{\int |S_L(\omega)*W(\omega)|_M w^h(\omega)d\omega}{\int w^h(\omega)d\omega}, \quad (15)$$

$$\overline{A_L^h(\omega)} = \frac{\int A_L^h(\omega) w^h(\omega)d\omega}{\int w^h(\omega)d\omega}. \quad (16)$$

To explain equation 13, we apply the average operator $\int[\cdot]w^l(\omega)d\omega \Big/ \int w^l(\omega)d\omega$ to 13 and obtain

$$\frac{\overline{A_L^l(\omega)}}{\overline{A_L^h(\omega)}} = \frac{\overline{|S_L(\omega)*W(\omega)|_M^l}}{\overline{|S_L(\omega)*W(\omega)|_M^h}}. \quad (17)$$

Equations 13 and 17 indicate, the amplitude $A_L^l(\omega)$ is built by adopt a theoretical shape function and assuming the low/high amplitude ratio is proportional to the low/high amplitude ratio of the source model. Substituting all quantities calculated in equations 10-13 into 6 and 7, and then into 4, we obtain $f_L(\omega)$. Followed by IFFT it to time domain, we have the short waveform $f_L(t)$.

To convert the entire seismogram into a new seismogram with low-frequency source, we use a moving time window $W(t-t')$ to continually sample the original seismogram. Each time, we repeat the above mentioned process to convert $f_H(t)$ into $f_L(t)$, and restore it to a new time series by aligning it to the sampling time t'. After sweep the entire seismogram, we obtain a new low-frequency seismogram. Typically, we use a 0.4 s long sampling window and each time move the window by 0.1 s. The redundancy makes the process robust.

Numerical examples

To validate the proposed method, we generate shot records with both 10-Hz and 3-Hz Ricker wavelets for the BP model. We convert the 10-Hz waveforms to 3-Hz waveforms and compare them with the waveforms actually calculated using 3-Hz Ricker wavelet. The result is shown in Fig 2, in which the solid lines are original 3-Hz seismograms and the dashed lines are converted from 10-Hz waveforms. We see the results are pretty consistent except for some minor deviations.

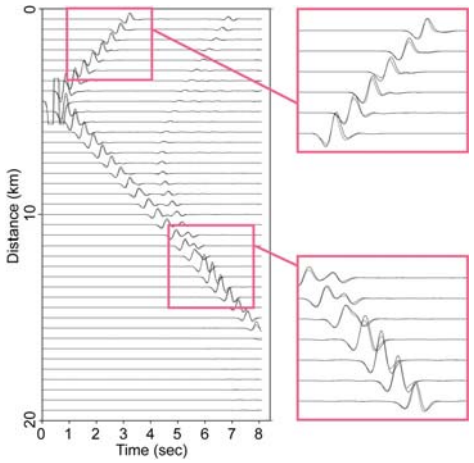

Fig 2. Comparison between the 10-Hz converted 3-Hz shot record (dashed lines) and the actually calculated 3-Hz shot record (solid lines).

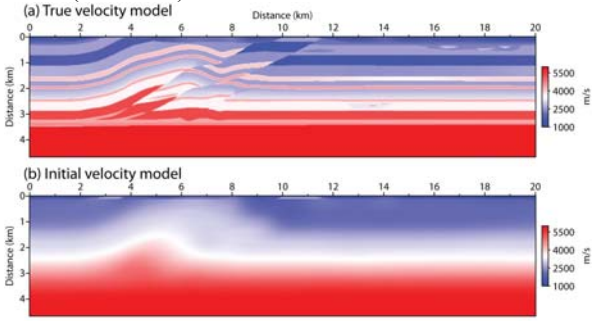

Fig 3. Overthrust velocity model, with (a) the original Overthrust model, and (b) the smoothed version used as the initial model.

As above mentioned, the low-frequency contents in the data make the FWI converging properly. To demonstrate this, we conduct the FWI for the Overthrust model using the time domain FWT package from SEISCOPE Consortium (http://seiscope.oca.eu/). The true velocity model is shown in Fig 3a. A synthetic data set with 5-Hz

DOI http://dx.doi.org/10.1190/segam2013-0451.1

Ricker source is generated using the true velocity model. Fifty-one shots and 401 evenly distributed surface receivers are used in the calculation. A smoothed version of the true velocity model shown in Fig 3b is used as the initial model to start the inversion. We calculate a total of 30 iterations to generate the result.

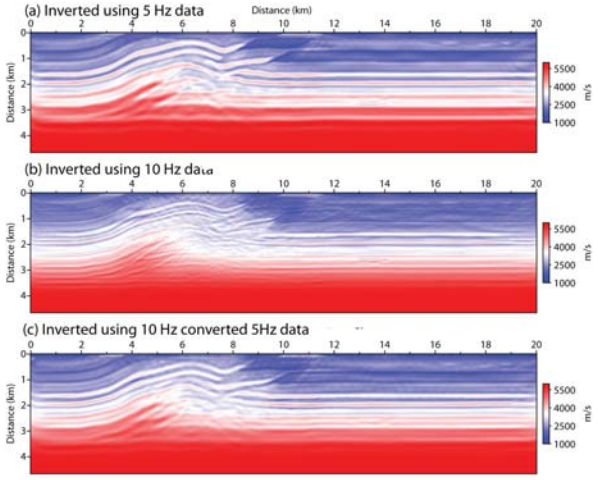

Fig 4. Comparison between the inverted results from different data sets, with (a) Inverted result from 5-Hz data, (b) inverted from 10-Hz data, and (c) inverted from 10-Hz converted 5-Hz data.

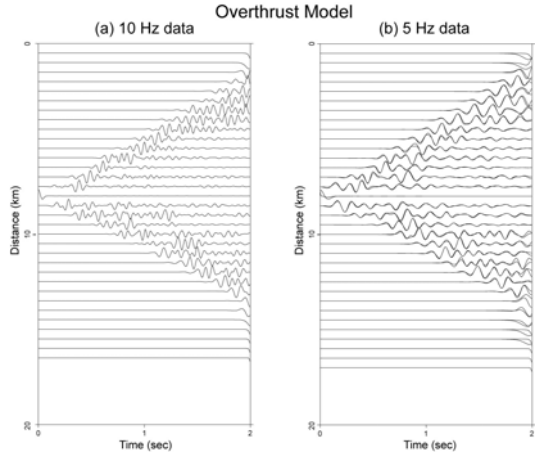

Fig 5. Comparison between the shot records calculated from Overthrust model, with (a) the 10-Hz shot record, and (b) comparison between the 10-Hz converted 5-Hz shot record (dashed lines) and the actually calculated 5-Hz shot record (solid lines). The errors at the beginning and end of the traces are caused by the truncation of the data.

The inverted result using the 5-Hz data is shown in Fig 4a. The result properly reveals features in the original velocity model. We then generate a 10-Hz synthetic data set for inversion and the result is shown in Fig 4b. Even with large number of iterations, the inversion still encounters convergence problem. Comparing the 5-Hz and 10-Hz results to the true velocity model, the 10-Hz result appearenly lacks long-wavelength information and seriously deviates from the true velocity. We then convert the 10-Hz data set into a 5-Hz data set. As an example, illustrated in Fig 5a is a shot record from the original 10-Hz data set. In Fig 5b, shown as dashed lines is the 10-Hz converted 5-Hz data set. As a comparison, we also include the actually calculated 5-Hz data set (solid lines) in Fig 5b. The converted 5-Hz data is very similar to the actually generated 5-Hz data except at the beginning and end of some traces where the original 10 Hz data is truncated. Shown in Fig 4c is the inverted velocity model using converted data. Compared to the 10-Hz result in Fig 5b, the 10-Hz converted 5-Hz data converge much better and the inverted velocity model is close to that using the actually calculated 5-Hz data.

Discussion and Conclusions

We propose a method to convert the high-frequency waveform into the low-frequency waveform. This method is validated for synthetic data set and successfully tested in the FWI. The proposed method is based on that the dispersion is weak at low frequencies. Thus the linear phase approximation can be adopted. For models generate strong dispersive waves at low frequencies, e.g., surface waves from shallow velocity gradient, this assumption may not be valid. When testing the synthetic data sets, we find it is relatively easier to convert 10-Hz data to 3-Hz data for the BP and Marmousi models. However, the error is large when convert the 10-Hz data to 3-Hz data for the Overthrust model, although it can be successfully converted to 5-Hz waveform. This may result from that the Overthrust model has strong shallow layering structure which generates abundant surface waves with their dominant frequency close to 3 Hz. The numerical tests are conducted for the synthetic data with known source time functions. For real field data, the source time function must be extracted from the data and additional errors may be involved.

Acknowledgement

The author thanks Dr. Jian Mao for discussions and help in calculations. This work is supported by the WTOPI Research Consortium at the University of California at Santa Cruz.

DOI http://dx.doi.org/10.1190/segam2013-0451.1

http://dx.doi.org/10.1190/segam2013-0451.1

EDITED REFERENCES

Note: This reference list is a copy-edited version of the reference list submitted by the author. Reference lists for the 2013 SEG Technical Program Expanded Abstracts have been copy edited so that references provided with the online metadata for each paper will achieve a high degree of linking to cited sources that appear on the Web.

REFERENCES

Ben-Hadj-Ali, H., S. Operto, and J. Virieux, 2008, Velocity model building by 3D frequency-domain, full-waveform inversion of wide-aperture seismic data: Geophysics, **73**, no. 5, VE101–VE117, http://dx.doi.org/10.1190/1.2957948.

Boonyasiriwat, C., P. Valasek, P. Routh, W. Cao, G. T. Schuster, and B. Macy, 2009, An efficient multiscale method for time-domain waveform tomography: Geophysics, **74**, no. 6, WCC59–WCC68, http://dx.doi.org/10.1190/1.3151869.

Bunks, C., F. M. Saleck, S. Zaleski, and G. Chavent, 1995, Multiscale seismic waveform inversion: Geophysics, **60**, 1457–1473, http://dx.doi.org/10.1190/1.1443880.

Fei, T. W., Y. Luo, F. Qin, and P. G. Kelamis, 2011, Full waveform inversion without low frequencies: A synthetic study, 82nd Annual International Meeting, SEG, Expanded Abstracts, http://dx.doi.org/10.1190/segam2012-0641.1.

Operto, S., J. Virieux, P. Amestoy, J.-Y. L'Excellent, L. Giraud, and H. B. H. Ali, 2007, 3D finite-difference frequency domain modeling of visco-acoustic wave propagation using a massively parallel direct solver: A feasibility study: Geophysics, **72**, no. 5, SM195–SM211, http://dx.doi.org/10.1190/1.2759835.

Sirgue, L., and R. G. Pratt, 2004, Efficient waveform inversion and imaging: A strategy for selecting temporal frequencies: Geophysics, **69**, 231–248, http://dx.doi.org/10.1190/1.1649391.